We are IntechOpen, the world's leading publisher of Open Access books Built by scientists, for scientists

6,900
Open access books available

185,000
International authors and editors

200M
Downloads

Our authors are among the

154
Countries delivered to

TOP 1%
most cited scientists

12.2%
Contributors from top 500 universities



WEB OF SCIENCE™

Selection of our books indexed in the Book Citation Index in Web of Science™ Core Collection (BKCI)

Interested in publishing with us?
Contact book.department@intechopen.com

Numbers displayed above are based on latest data collected.
For more information visit www.intechopen.com



Chapter

Metal Oxide Nanowires as Building Blocks for Optoelectronic Devices

Andreea Costas, Nicoleta Preda, Camelia Florica and Ionut Enculescu

Abstract

Metal oxide nanowires have become the new building blocks for the next generation optoelectronic devices due to their specific features such as quantum confinement and high aspect ratio. Thus, they can be integrated as active components in diodes, field effect transistors, photodetectors, sensors, solar cells and so on. ZnO, a n-type semiconductor with a direct wide band gap (3.3 eV) and CuO, a p-type semiconductor with a narrow band gap (1.2–1.5 eV), are two metal oxides which were recently in the spotlight of the researchers for applications in the optoelectronic devices area. Therefore, in this chapter we focused on ZnO and CuO nanowires, the metal oxides nanowire arrays being prepared by straightforward wet and dry methods. Further, in order to emphasize their intrinsic transport properties, lithographic and thin films deposition techniques were used to integrate single ZnO and CuO nanowires into diodes and field effect transistors.

Keywords: metal oxide nanowire arrays, single ZnO and CuO nanowires, lithographic techniques, diodes, field effect transistors

1. Introduction

Over the last decades, metal oxide nanowires, one dimensional nanostructures characterized by a high aspect ratio [1], have gained a special interest owed among others to their large specific area given by the size effects. This feature is responsible for their high sensitivity that is very important in a wide range of applications in optoelectronics [2], electrochemical sensors [3], spintronics [4], photocatalysis [5], noninvasive medical diagnosis [6], drug delivery [7], etc. Thus, due to their high sensitivity, metal oxide nanowires can detect even a single molecule, or even mechanical, optical or electrical signals [8–10]. For example, the size of biological molecules, such as proteins and nucleic acids, is comparable to the size of nanostructures, therefore any interaction between these molecules should induce major changes in the properties of the nanowires. Consequently, the metal oxide nanowires can be regarded as the perfect candidates for integration as single components in diodes [11], field effect transistors [12, 13], advanced biosensors [14], photodetectors [15], light emitting diodes [16], solar cells [17], magnetoresistive sensors [18], etc.

The preparation methods represent the key factor in order to obtain metal oxide nanowires with tunable dimensions and tailored physico-chemical properties. To date, many preparation approaches were used for preparing arrays of metal oxide nanowires, such as template electrodeposition [19], electroless deposition [20], sol–gel [21], chemical bath deposition [22], hydrothermal growth [23], pulsed laser deposition [24], chemical vapor deposition [25], atomic layer deposition [26], lithographic techniques [27], etc. Among them, chemical synthesis carried out in water as a reaction medium is a simple wet preparation route, easy to process and suitable for large-scale synthesis of metal oxide powders consisting in micro- and nano-structures with different morphologies featured by a good crystallinity [13, 28, 29]. Another preparation method, thermal oxidation in air is a relatively facile dry, low-cost, non-hazardous and high throughput approach that can be used at a large-scale to obtain metal oxides nanostructures of a high purity and crystallinity [13]. Using thermal oxidation in air to obtain arrays of metal oxide nanowires, the nanowires length, diameter and density can be easily controlled by modifying the parameters involved in the thermal oxidation in air process, such as: the heating rate, the annealing temperature and the time of the treatment [30].

Zinc oxide (ZnO) is an interesting eco-friendly and versatile metal oxide, suitable for many applications due to its remarkable physico-chemical properties. Being an n-type semiconductor with a direct band gap (3.37 eV), with an excitonic binding energy of 60 meV, it can be easily integrated in optoelectronic devices such as photodetectors [15], light emitting diodes [31], solar cells [32]. Additionally, its flexibility in terms of nanostructure morphology (nanowires, nanotubes, nanofibers, nanorods, nanoneedles, hexagonal nanoprisms, nanoflowers, rings, etc.) [33, 34] offers another important advantage for applications in sensors [35], photocatalysis [36], as well as in surfaces with self-cleaning properties [37].

Copper oxide (CuO) is a p-type semiconductor easy to prepare, with a high stability, having an indirect narrow band gap (1.2–1.8 eV). This metal oxide can be implemented in various applications such as: solar cells [38], field effect transistor [11], gas sensors [39], photocatalysis [40], water purification [41], etc. Being also an antiferromagnetic material below 220 K with a local magnetic moment of about 0.6 μ_B, CuO was also investigated for application in magnetic storage units [42].

In this chapter, we present our research regarding the preparation and complex characterization of metal oxide nanowire arrays by wet (chemical synthesis in aqueous solution) and dry (thermal oxidation in air) approaches. In addition, electronic devices based on single metal oxide nanowires were developed and analyzed in terms of electrical characterization. Further, lithographic techniques such as photolithography, electron beam lithography and focused ion beam induced deposition, combined with radio-frequency magnetron sputtering and thermal vacuum evaporation were used for fabricating electronic devices like diodes and field effect transistors based on single metal oxide (ZnO or CuO) nanowires. In addition, the electrical properties of the electronic devices based on single metal oxide nanowires prepared by wet and dry methods were analyzed and discussed.

2. Lithographic techniques

Lithographic techniques are mainly used in modern semiconductor manufacturing industry, in micro- and nano-fabrication to pattern thin films with specific geometries integrated into electronic devices. Lithographic techniques are subsequently divided according to the targeted application into: photolithography, electron beam lithography, focused ion beam induced deposition, extreme UV lithography, nanoimprint lithography, colloidal lithography, soft lithography, and

many others. In the following, the techniques involved in the fabrication of our electronic devices based on single metal oxide nanowires are briefly described.

2.1 Photolithography

Photolithography is a conventional lithographic process in which specific geometric shapes drawn on a photomask are transferred to the desired substrate by means of light in the UV range, using a lamp that emits UV light of a certain wavelength and a polymer that has a photoactive component sensitive to the UV light named photoresist. In this case, the resolution is limited by the wavelength used and by the type of the aligner. In our case, the photolithography was involved in the fabrication of Ti/Au metallic interdigitated electrodes onto Si/SiO_2 wafers. The main steps of the process being: cleaning of the Si/SiO_2 wafers, deposition of the primer and the photoresist by centrifugation, baking of the deposited layer, the mask alignment, the UV exposure, baking after UV irradiation, the UV exposure through clear mask, the development process and the deposition of Ti and Au thin films using radio-frequency (RF) magnetron sputtering and thermal vacuum evaporation, respectively.

2.2 Electron beam lithography

Electron beam lithography (EBL) is a lithographic technique that uses a high-voltage accelerated electron beam to directly pattern a substrate without the need of a mask. In this process, the electron beam irradiates a thin layer of electron-sensitive polymer which was previously deposited on the substrate. During the exposure, the polymer (electron beam resist) bonds break and thus after the lift-off process, the appropriate geometric configuration is obtained. This technique has a high resolution, that can be used in nanoscale electronics, optoelectronics and photonics. In our case, in order to contact single nanowires using EBL, the first step is to transfer the nanowires between the metallic interdigitated electrodes. Further, a layer of electron beam resist –polymethyl methacrylate (PMMA) is deposited on the sample. Then, the desired contacts are designed into a CAD program and exposed with the electron beam. After the development process, the Ti and Au or Pt thin films are deposited by RF magnetron sputtering and thermal vacuum evaporation, respectively. Finally, the lift-off process removes the excess metal and the Ti/Au contacts are obtained.

2.3 Focused ion beam induced deposition

Focused ion beam induced deposition (FIBID) is a lithographic technique that uses a highly focused ion beam of gallium ions (Ga^+), a gas injection system and an organometallic precursor gas to deposit a metallic thin film without the need of a mask onto a substrate. In our case, similar to the EBL lithographic process, to contact single metal oxide nanowires by FIBID, the first step is to place the nanowires between the metallic interdigitated electrodes. Afterwards, the future Pt contacts are designed into a CAD program. During the deposition of the Pt contacts, an injector needle is placed very near to the substrate and upon the interaction between the organometallic compound with the ion beam, the precursor molecules are decomposed into a platinum layer and a volatile organic compound exhausted into the vacuum system. FIBID deposition is limited by the organometallic precursor gas and by the delivery rate of the gas. The deposition of a Pt contact by FIBID leads to the deposition of a carbon amorphous matrix that incorporates Pt nanoparticles implanted with Ga^+ ions.

3. Metal oxide nanowires: Influence of the preparation method type (wet or dry) on their structural, morphological and optical properties

Arrays of metal oxides (ZnO and CuO) nanowires were prepared involving two simple cost-effective wet and dry approaches: chemical synthesis in aqueous solution and thermal oxidation in air.

3.1 CuO nanowires

CuO nanowire arrays obtained by a wet method were chemically synthesized in aqueous solution based on the procedure described in Ref.s [43]. Thus, 0.0045 mol NH_4OH in 30 ml aqueous solution and 0.007 mol NaOH in 6 ml aqueous solution were added, under vigorous stirring, in a glass beaker with 100 ml aqueous solution containing 0.004 mol $CuSO_4$. The beaker was covered and stored for 7 days without stirring at ambient temperature. The precipitate was collected through centrifugation, washed several times with water and dried at room temperature.

Figure 1(a) illustrates a SEM image of the CuO nanowires chemically synthesized in aqueous solution, indicating that these nanowires have a cylindrical shape, lengths up to 2 μm and diameters of about 40 nm. The XRD pattern of the prepared CuO nanowires (**Figure 1(b)**) evidences peaks corresponding to the Miller indexes of the reflecting planes for CuO in a monoclinic phase (JCPDS reference code 00–048-1548). Based on the reflectance spectrum of the obtained CuO nanowires (**Figure 1(c)**), the band gap value was estimated as being around 1.6 eV, in agreement with previously reported data for CuO nanowires [44].

Arrays of CuO nanowire were prepared also by a dry method, using thermal oxidation in air according to the procedure given in Ref.s [11, 30]. Briefly, metallic substrates consisting in 2 cm^2 copper foils were cleaned in ultrasonic bath with acetone and isopropyl alcohol and then annealed in air for 24 h at 400°C, 500°C and 600°C in a convection oven.

The SEM images in cross-sectional view of the annealed Cu foils (**Figure 2(a), (c), (e)**) revealed that there are three distinct regions with different morphologies from the bottom up: the Cu foil, a Cu_2O thin film and the CuO nanowire arrays. Moreover, the SEM images in plan-view of the CuO nanowire arrays (**Figure 2(b), (d), (f)**) prepared by thermal oxidation in air at different temperatures disclose that the increase of the annealing temperature favors a higher density and a larger diameter of the CuO nanowires. Thus, the diameters and lengths of the CuO nanowires can be tuned as a function of the applied annealing temperatures. At 400°C, there is a low density of nanowires with diameters of

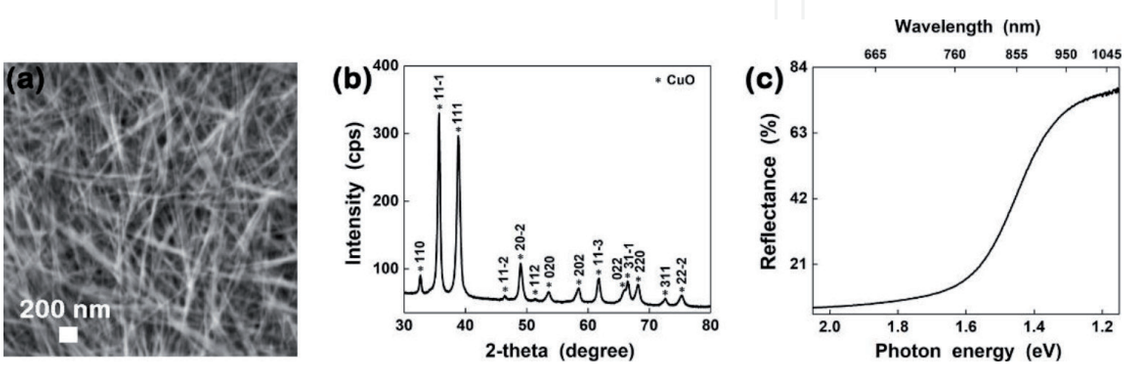


Figure 1.
(a) SEM image, (b) XRD pattern and (c) reflectance spectrum of the CuO nanowire arrays obtained by chemical synthesis in aqueous solution.

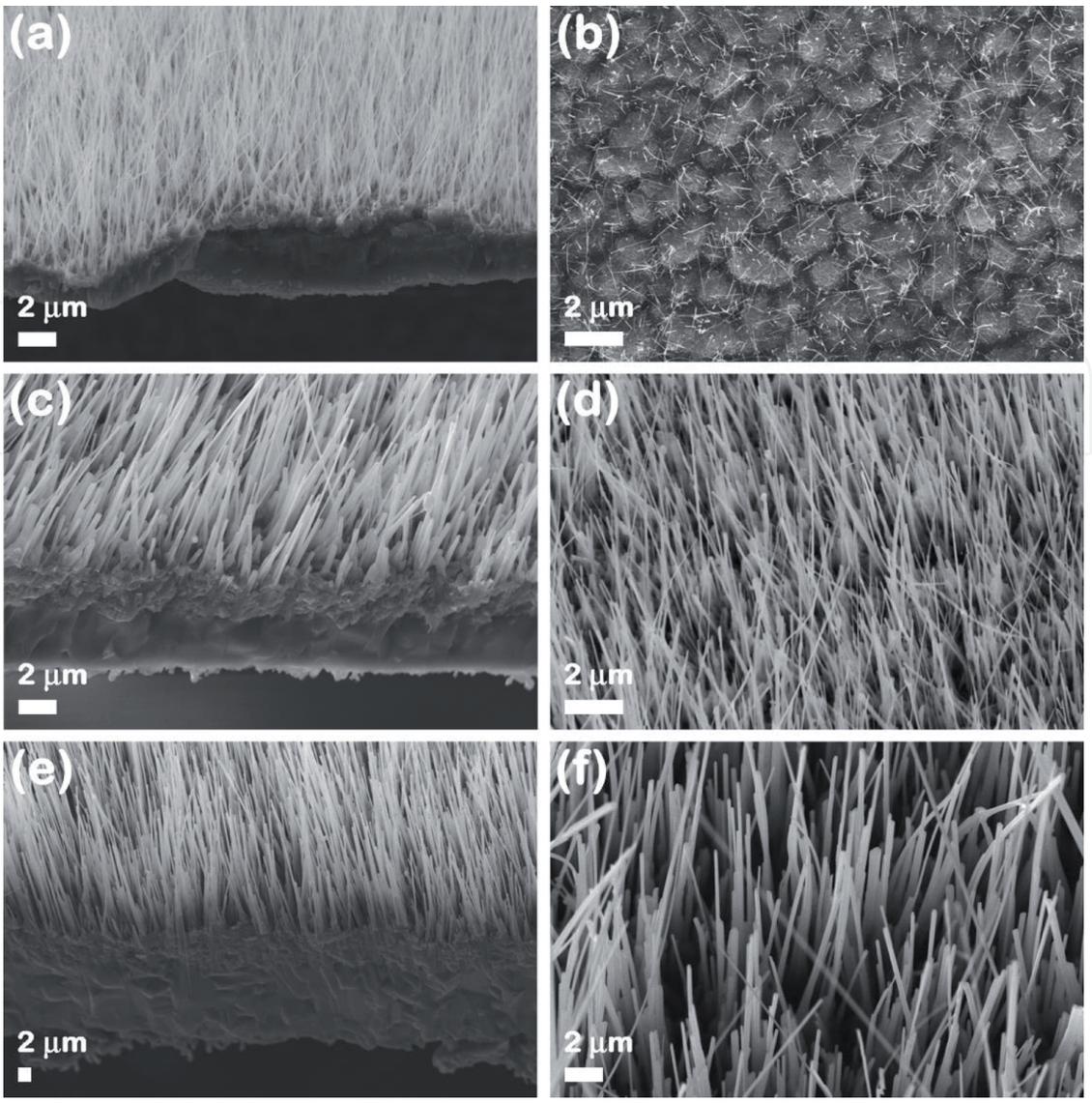


Figure 2.
SEM images of the CuO nanowire arrays prepared by thermal oxidation in air at (a), (b) 400°C, (c), (d) 500°C and (e), (f) 600°C.

about 40 nm and lengths up to 1 μm. At 500°C, there is a high density of nanowires with diameters of about 60 nm and lengths up to 30 μm. Also, at 600°C, there is a much higher density of nanowires with diameters of about 100 nm and lengths up to 30 μm.

The structural properties of the Cu foils thermally oxidized in air at different temperatures consisting in the XRD patterns (**Figure 3(a), (c), (e)**) evidence the presence of diffraction peaks assigned to the Miller indexes of the reflecting planes for three crystalline phases: Cu in face-centered-cubic phase (JCPDS reference code 00–004-0836), Cu_2O in cubic phase (JCPDS reference code 01–071-3645) and CuO in monoclinic phase (JCPDS reference code 00–048-1548). These results are in accordance with the data obtained for the CuO nanowire arrays in the cross-sectional SEM images (**Figure 2(a), (c), (e)**) in which there were clearly observed three distinct areas with different morphologies.

The band gap values for the CuO nanowire arrays obtained by thermal oxidation in air at various temperatures were assessed based on the reflectance spectra (**Figure 3(b), (d), (f)**) as being around 1.6 eV, in agreement with data previously reported in the literature for CuO nanowires [44].

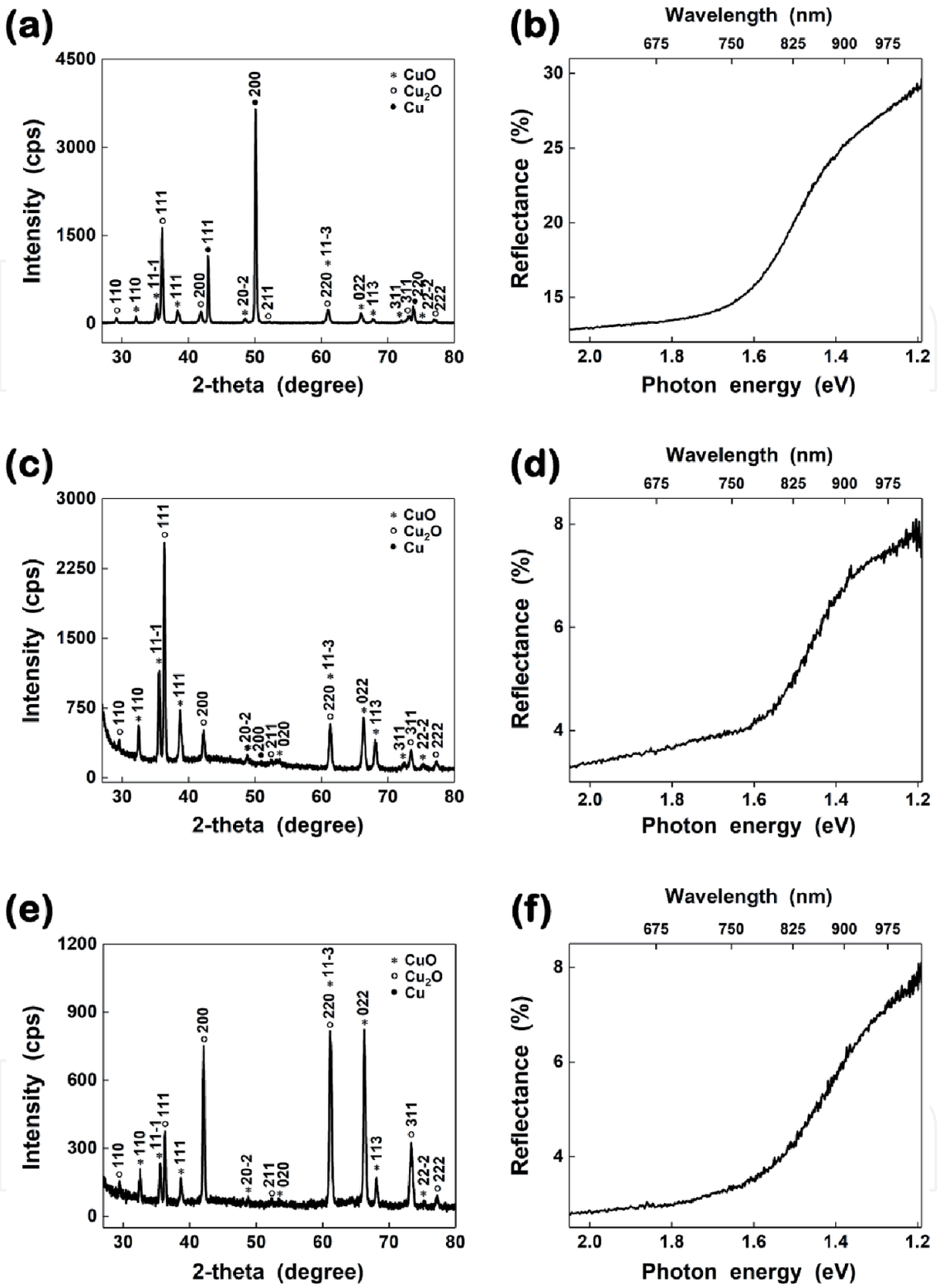


Figure 3.
(a), (c), (e) XRD patterns and (b), (d), (f) reflectance spectra of the CuO nanowire arrays prepared by thermal oxidation in air at (a), (b) 400°C, (c), (d) 500°C and (e), (f) 600°C.

3.2 ZnO nanowires

ZnO nanowire arrays were chemically synthesized in aqueous solution based on the procedures described in Ref.s [13, 28, 29]. Thus, a glass beaker with 300 ml aqueous solution containing 0.1 mmol $Zn(NO_3)_2$ and 0.1 mmol $(CH_2)_6N_4$ was covered and placed in a hot air oven, preheated at 90°C. After 5 h, the substrates, Si/SiO_2 pieces coated with a thin Ti/Au layer, were dipped and kept in the aqueous

solution for 2 days. The Ti layer behaves as an adhesion promoter for the Au layer, which acts as a nucleation layer assisting the growth of ZnO nanowires.

The morphological properties of the ZnO nanowire chemically synthesized in aqueous solution are presented in **Figure 4(a)**, the SEM image revealing that the nanowires have a cylindrical shape with lengths up to 10 μm and very thin diameters of about 20 nm. The XRD pattern of the ZnO nanowires obtained by a wet method (**Figure 4(b)**) evidences peaks corresponding to the Miller indexes of the reflecting planes for ZnO crystalized in a hexagonal wurtzite phase (JCPDS reference code 00–036-1451).

The optical properties of the ZnO nanowire arrays were analyzed by reflectance and photoluminescence measurements (**Figure 4(c)** and **(d)**). From the reflectance spectrum, a band gap value was estimated of about 3.3 eV, similar with the values reported in the literature for ZnO nanowires [13]. The photoluminescence spectrum of the obtained ZnO nanowires (**Figure 4(d)**) disclose only the presence of a broad, intense emission band, centered at approximately 2.2 eV. Usually, for the ZnO nanowires synthesized in water, this broad emission band from the visible region is linked to the higher concentrations of point defects like: zinc vacancy, interstitial zinc, oxygen vacancy, interstitial oxygen, hydroxyl group, etc. [13].

Arrays of ZnO nanowire obtained by a dry route were prepared according to the method from references [13, 37]. Thus, 2 cm^2 zinc foils were cleaned in an ultrasonic bath with acetone and isopropyl alcohol and thermally oxidized in air for 24 h at 400°C, 500°C and 600°C in a convection oven.

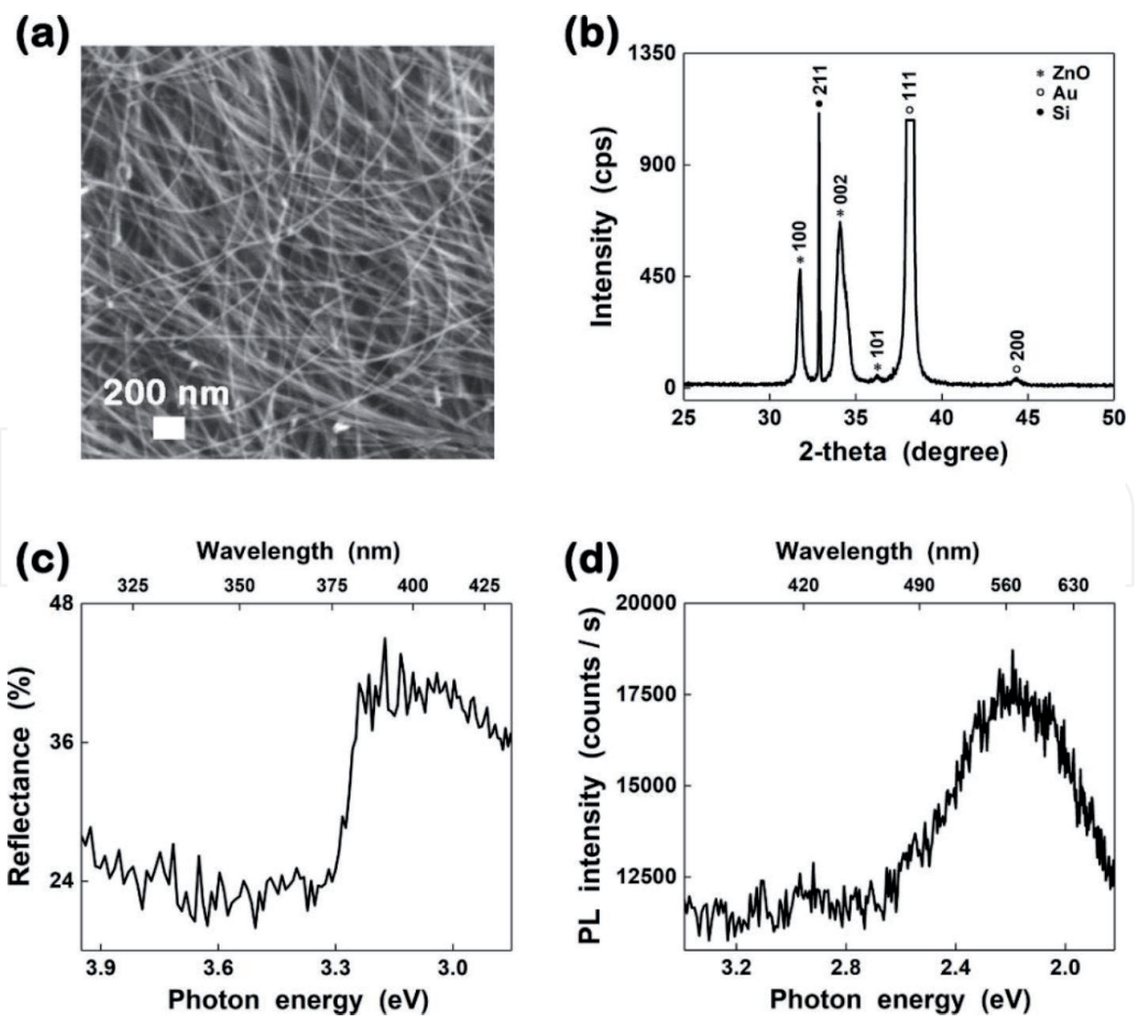


Figure 4.
(a) SEM image, (b) XRD pattern, (c) reflectance spectrum and (d) photoluminescence spectrum of the ZnO nanowire arrays obtained by chemical synthesis in aqueous solution.

The SEM images in cross-sectional view of the thermally oxidized Zn foils (**Figure 5(a), (c), (e)**) show that there are two distinct regions with different morphologies: one as a film, attributed to the metallic Zn and the second one, as nanowire arrays, associated to ZnO.

Additionally, similar with the CuO nanowire arrays obtained by a dry technique, the SEM images in plan-view of the ZnO nanowire arrays prepared by thermal oxidation in air at different temperatures (**Figure 5(b), (d), (f)**) evidence that the increase of the annealing temperature favors a higher density and a larger diameter of the ZnO nanowires. Hence, at 400°C there is a low density of nanowires with diameters of about 20 nm and lengths up to 1 μm, while at 500°C and 600°C there is a much higher density of nanowires with diameters of about 30 nm (500°C) and 60 nm (600°C) and lengths up to 30 μm.

The XRD patterns of the Zn foils thermally oxidized in air at different temperatures (**Figure 6(a), (d), (g)**) disclose the presence of diffraction peaks assigned to the Miller indexes of the reflecting planes for two crystalline phases: Zn in hexagonal phase (JCPDS reference code 00–004-0831) and ZnO crystalized in a hexagonal wurtzite phase (JCPDS reference code 00–036-1451). The structural properties are in agreement with the two distinct regions with different morphologies observed in

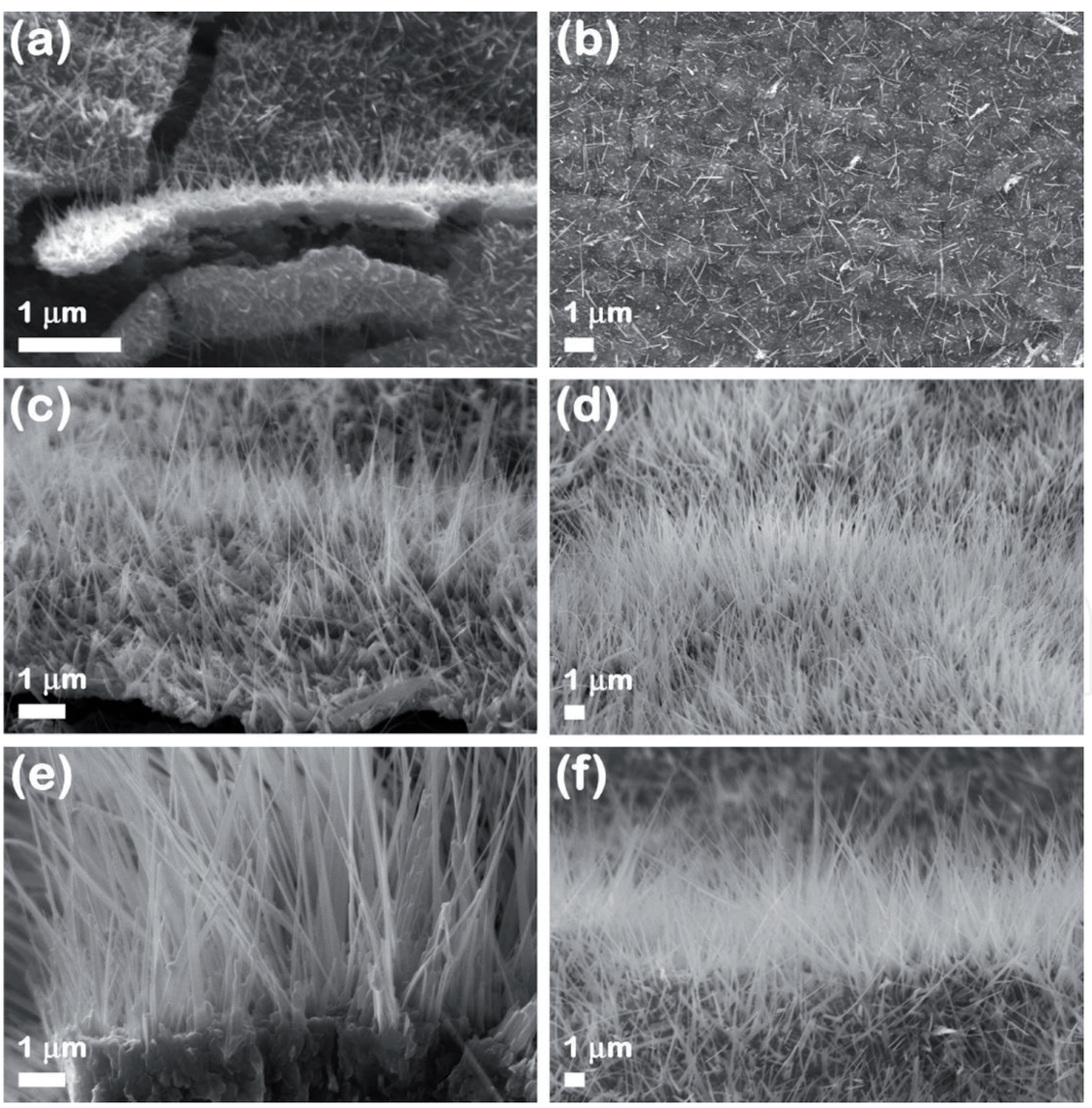


Figure 5.
SEM images of the ZnO nanowire arrays prepared by thermal oxidation in air at (a), (b) 400°C, (c), (d) 500°C and (e), (f) 600°C.

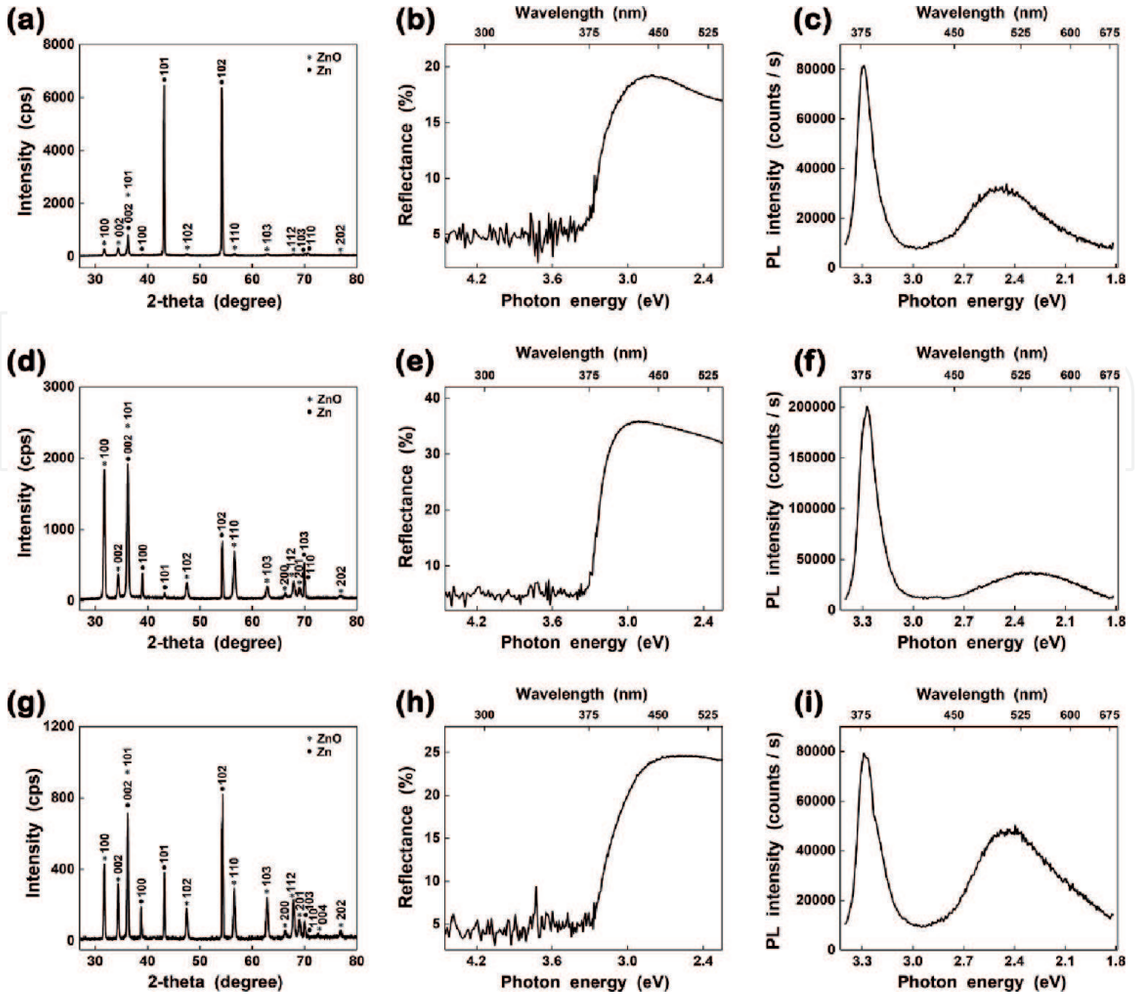


Figure 6.
(a), (d), (g) XRD patterns, (b), (e), (h) reflectance spectra and (c), (f), (i) photoluminescence spectra of the ZnO nanowire arrays prepared by thermal oxidation in air at (a), (b), (c) 400°C, (d), (e), (f) 500°C and (g), (h), (i) 600°C.

the cross-sectional SEM images (**Figure 5(a), (c), (e)**) for the ZnO nanowire arrays.

Based on the reflectance spectra of the ZnO nanowire arrays obtained by thermal oxidation in air at different temperatures (**Figure 6(b), (e), (h)**), the band gap values were estimated as being at about 3.3 eV, in accordance with data previously reports for ZnO nanowires [13].

The photoluminescence spectra of the ZnO nanowires obtained by a dry method at different annealing temperatures (**Figure 6(c), (f), (i)**) reveal the presence of two emission bands: one intense, sharp and centered at approximately 3.3 eV in the UV region and another one, weak and broad, centered at approximately 2.3 eV in the visible region. The sharp emission band in the UV region is related to the band-edge emission and the one in the visible region is linked to the various type of point defects [13].

4. Electronic devices (diodes and field effect transistors: FETs) based on single metal oxide nanowires

In order to evaluate the electrical properties and to integrate single CuO or ZnO nanowires obtained by wet (chemical synthesis in aqueous solution) and dry (thermal oxidation in air) methods into electronic devices like diodes or field effect

transistors, lithographic techniques and thin films deposition techniques were employed.

Firstly, photolithography together with radio-frequency magnetron sputtering and thermal vacuum evaporation were used to pattern Si/SiO_2 wafers with Ti/Au (10 nm/100 nm) metallic interdigitated electrodes systems. Subsequently, suspensions of CuO or ZnO nanowires in ultrapure isopropyl alcohol are prepared by ultrasonication and then drop-cast onto the Si/SiO_2 substrates patterned with Ti-Au metallic interdigitated electrodes. Afterwards, single CuO or ZnO nanowires are contacted by EBL, FIBID or EBL combined with FIBID. **Figure 7(a)** illustrates a SEM image of a Si/SiO_2 substrate patterned with Ti/Au metallic interdigitated electrode system, while **Figure 7(b)** presents a SEM image of Ti/Au metallic interdigitated electrodes having metal oxide nanowires, transferred by drop-casting, between the Ti/Au electrodes.

The electrical measurements of the single CuO or ZnO nanowires contacted by lithographic techniques were carried out at room temperature in a typical two-points configuration for diodes and a three-points configuration for FETs.

4.1 Diodes and FETs based on single CuO nanowires

In the following, CuO nanowires prepared by thermal oxidation in air at 500°C were used to develop diodes and FETs based on single CuO nanowires, these nanowires being chosen owed to the smaller diameter of about 60 nm and the lengths of about 30 μm for the nanowires.

Single CuO nanowire based Schottky diodes were fabricated by contacting single CuO nanowires at one end with Ti/Au by EBL and at the other end with Pt using FIBID. This outcome can be explained considering that a Pt–CuO nanowire structure exhibits an Ohmic behavior, and that a CuO nanowire–Ti/Au structure discloses a Schottky rectifying behavior [11]. Thus, **Figure 8(a)** presents a SEM image of a single CuO nanowire prepared by thermal oxidation in air and contacted at one end with Ti/Au (100 nm/300 nm) by EBL, RF magnetron sputtering and thermal vacuum evaporation and at the other end with Pt (300 nm) by FIBID, evidencing a distance between the metallic contacts of about 11 μm. **Figure 8(b)** displays the EDX elemental mapping analysis of the metallic electrodes that contact

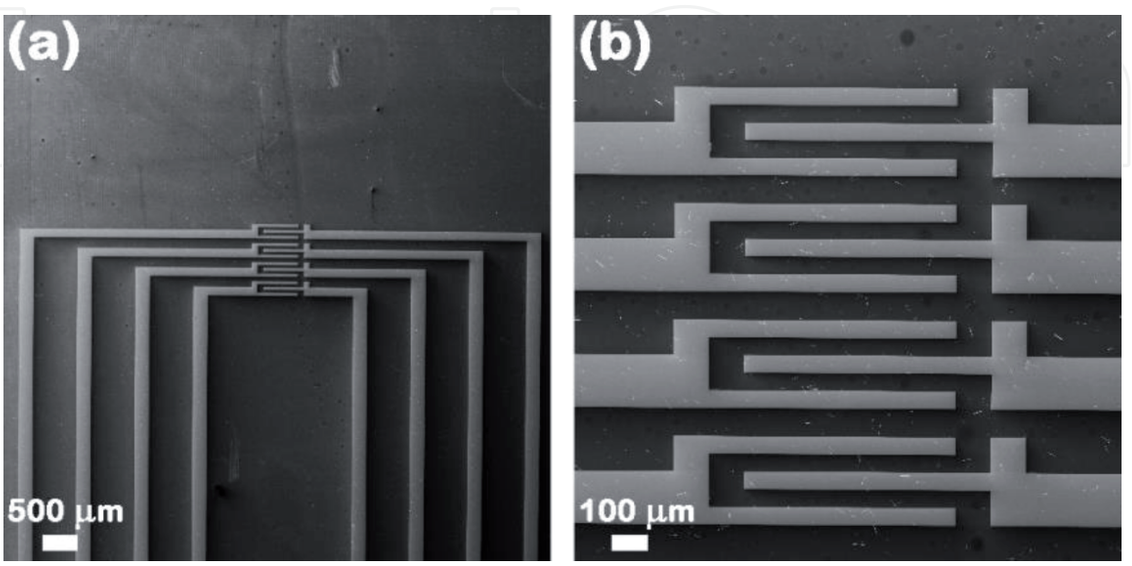


Figure 7.
(a) SEM image of a Si/SiO_2 substrate containing Ti/Au metallic interdigitated electrodes and (b) SEM image of Ti/Au metallic interdigitated electrodes having metal oxide nanowires placed between the Ti/Au electrodes.

the nanowire to the metallic interdigitated electrodes, confirming the presence of Ti and Au elements in the case of EBL and Pt for FIBID. The current–voltage characteristics of a single CuO nanowire contacted by EBL and FIBID (**Figure 8(c)**) reveal a rectifying Schottky behavior, typical for a Schottky diode [11]. Moreover, the values of the specific parameters for diodes were estimated from the current–voltage dependence to be: I_{ON}/I_{OFF} ratio $\approx 10^3$ and the ideality factor $n \approx 1.8$, being in accordance with data reported in the literature [11].

In order to develop FETs based on single CuO nanowires, FIBID was used to contact single CuO nanowires at both ends of the nanowire with Pt (300 nm), the SEM image of a single CuO nanowire contacted by this technique being illustrated in **Figure 9(a)**. The current–voltage characteristic of a single CuO nanowire contacted by FIBID (**Figure 9(b)**) evidences a linear dependence, indicating an Ohmic contact formed between the CuO nanowire and Pt electrodes.

Figure 10(a) and **(b)** present a SEM image and the corresponding EDX mapping, proving the presence of the Pt element into the source and drain electrodes and Cu in the CuO nanowire. The length of the p-type semiconductor channel between the source and drain is about 8 μm. The output characteristics (**Figure 10(c)**) exhibit an increase in the source-drain current towards higher negative gate voltages, typical for a p-type semiconductor channel. Also, it can be noticed a change in the shape of the output characteristic at −12 V applied gate voltage, indicating the saturation region of the FET. The semilogarithmic plot of the transfer characteristic of the single CuO nanowire based FET (**Figure 10(d)**) disclose an I_{ON}/I_{OFF} ratio $\approx 10^3$, in agreement with data reported in the literature for FETs based on single nanowires [11].

4.2 Diodes and FETs based on single ZnO nanowires

In the fabrication of diodes and FETs based on single ZnO nanowires were used ZnO nanowires prepared by thermal oxidation in air at 500°C, these being chosen due to their smaller diameter of about 30 nm and the lengths of about 30 μm and also ZnO nanowires chemically synthesized in aqueous solution.

In order to develop diodes based on ZnO nanowires obtained by a dry method, single ZnO nanowire were contacted at the both ends of the nanowire Ti/Au by EBL. Hence, **Figure 11(a)** and **(b)** displays two SEM images, at different magnifications, of a single ZnO nanowire prepared by thermal oxidation in air and contacted at both ends with Ti/Pt (100 nm/200 nm) by EBL and RF magnetron sputtering, evidencing a distance between the metallic contacts of about 2 μm. The current–voltage measurement of a single ZnO nanowire contacted by EBL (**Figure 11(c)**) exhibits a non-liniar symmetrical shape indicating a structure having two back-to-back Schottky diodes, similar type of behavior being reported in the literature [45].

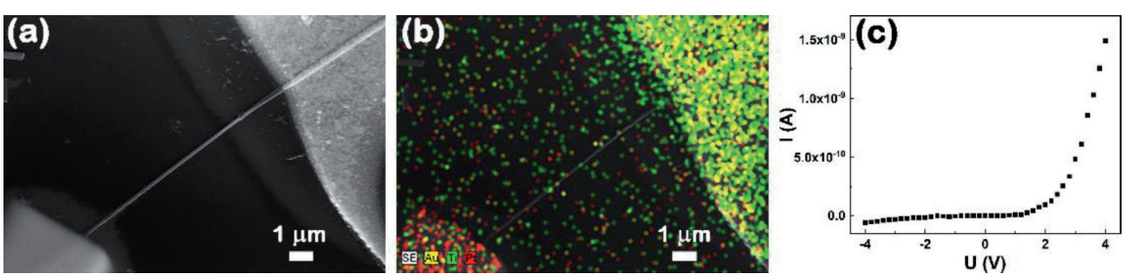


Figure 8.
(a) SEM image, (b) EDX elemental mapping and (c) current–voltage characteristic of a single CuO nanowire prepared by a dry method and contacted by EBL and FIBID.

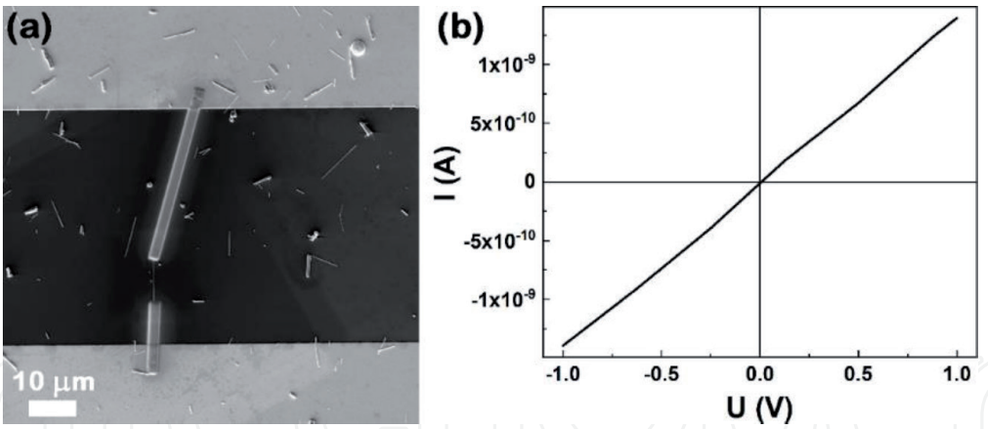


Figure 9.
(a) SEM image and (b) current–voltage of a single CuO nanowire prepared by a dry method and contacted by FIBID.

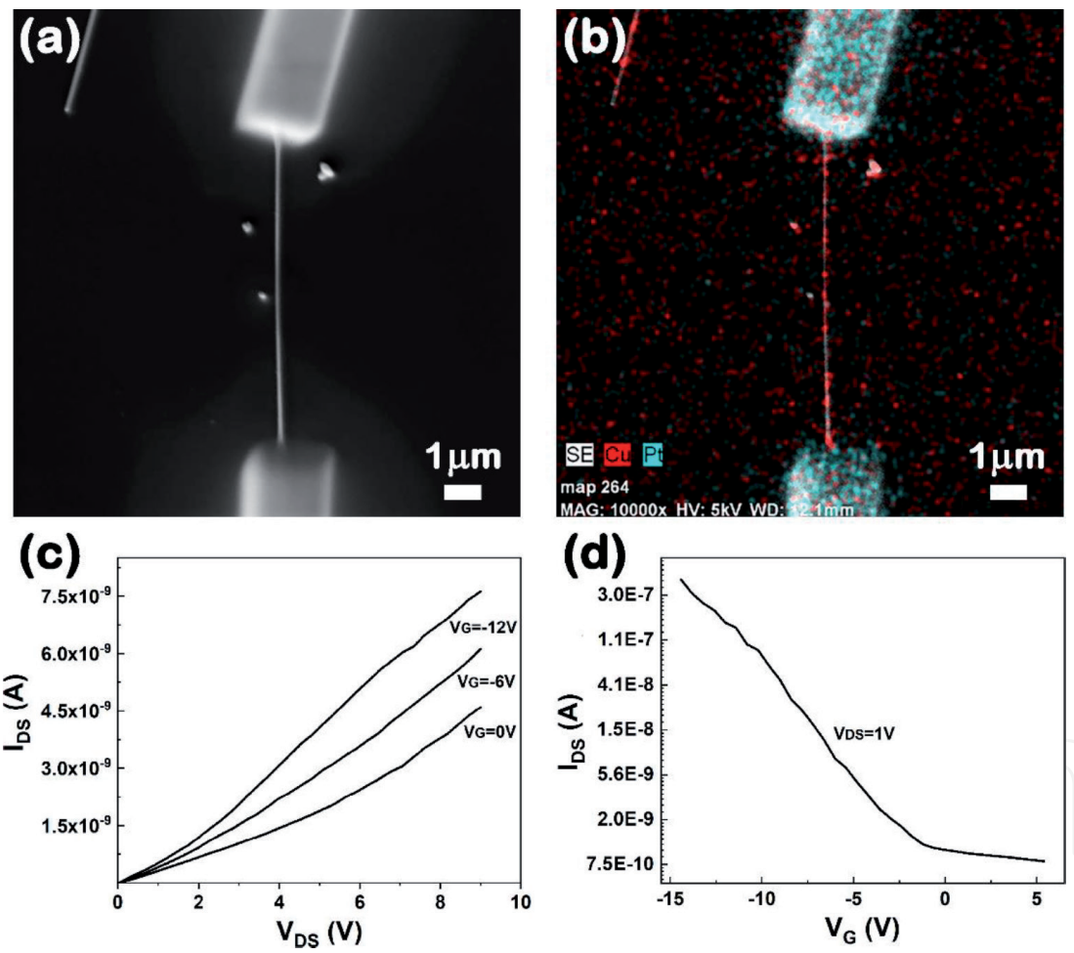


Figure 10.
(a) SEM image, (b) EDX elemental mapping, (c) output and (d) transfer characteristics of a FET based on a single CuO nanowire prepared by a dry method and contacted by FIBID.

FETs based on single ZnO nanowires prepared by a dry method were fabricated by contacting single ZnO nanowires at both ends with Ti/Au (100 nm/300 nm) by EBL, RF magnetron sputtering and thermal vacuum evaporation, the SEM image of a single ZnO nanowire contacted by EBL being illustrated in **Figure 12(a)**. The current–voltage dependence of a single ZnO nanowire contacted by EBL (**Figure 12(b)**) put in evidence a linear shape, typical for an Ohmic contact formed between the ZnO nanowire and the two Ti/Au contacts.

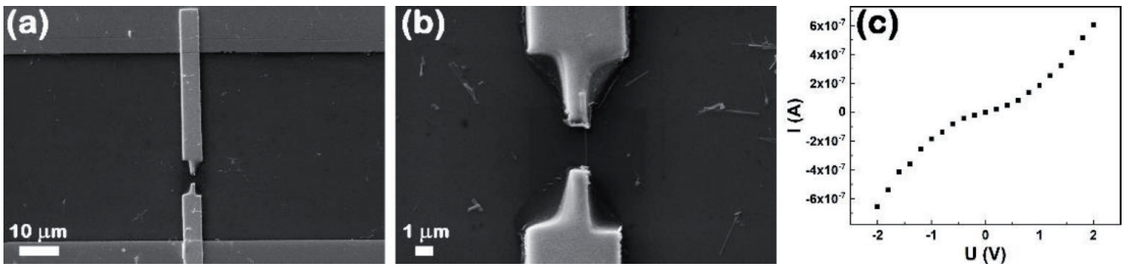


Figure 11.
(a), (b) SEM images and (c) current–voltage characteristic of a single ZnO nanowire prepared by a dry method and contacted by EBL.

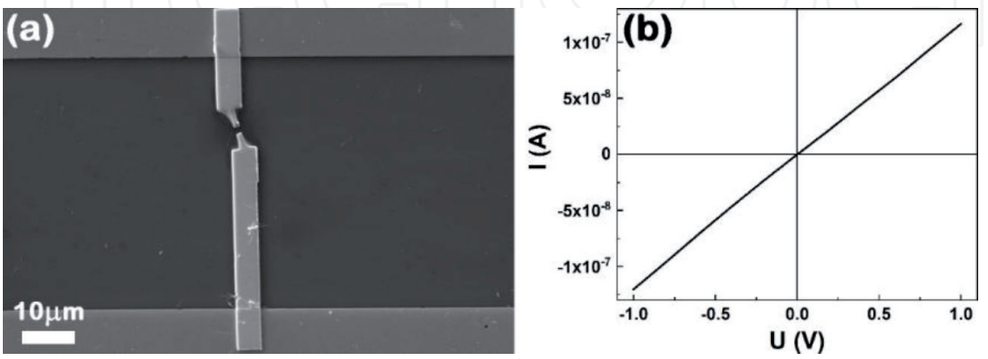


Figure 12.
(a) SEM image and (b) current–voltage characteristic of a single ZnO nanowire prepared by a dry method and contacted by EBL.

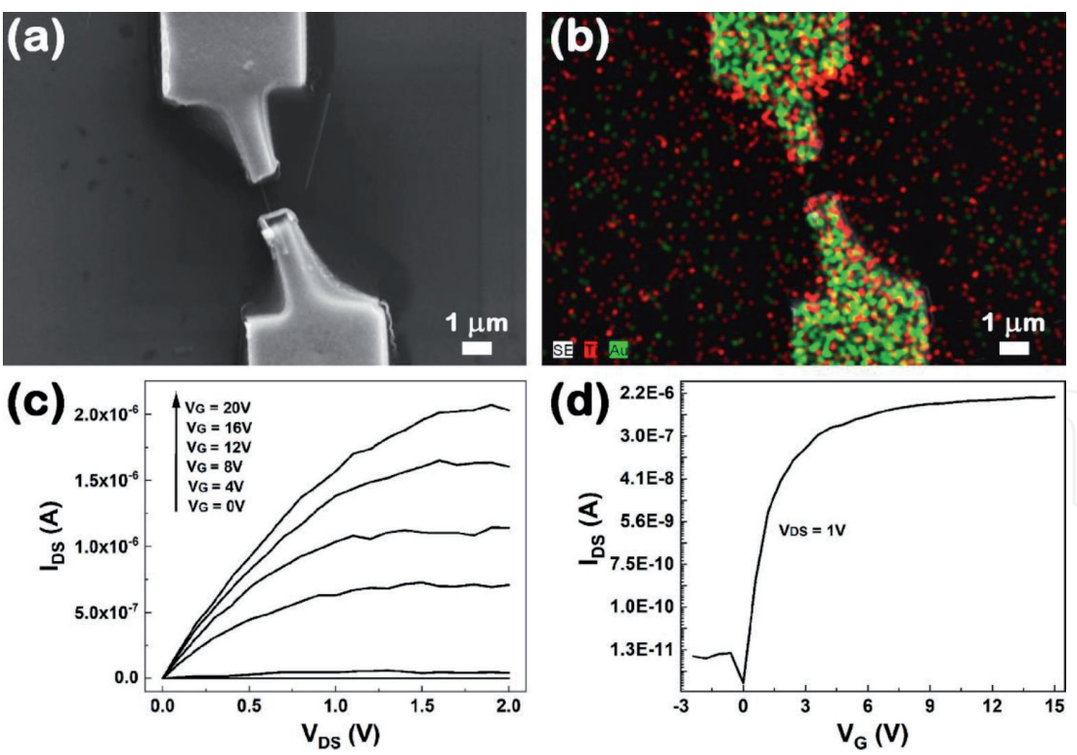


Figure 13.
(a) SEM image, (b) EDX elemental mapping, (c) output and (d) transfer characteristics of a FET based on a single ZnO nanowire prepared by a dry method and contacted by EBL.

Figure 13(a) displays a SEM image of a single ZnO nanowire contacted by EBL, indicating that the length of the n-type semiconductor channel between the source and drain is about 1 μm. The equivalent EDX mapping image (**Figure 13(b)**) proves

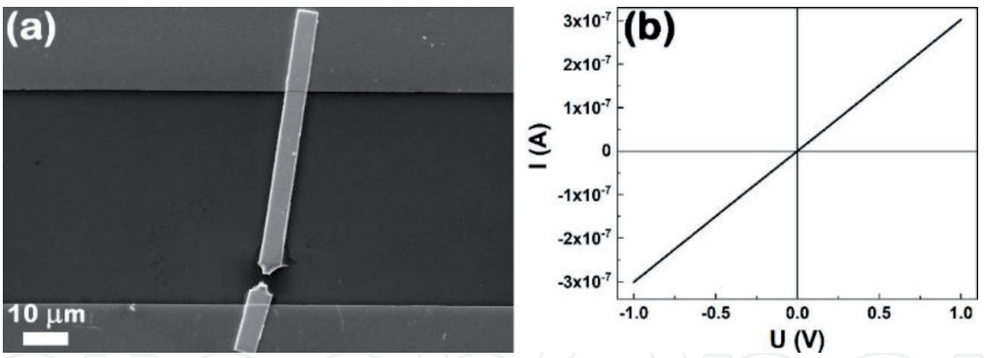


Figure 14.
(a) SEM image and (b) current–voltage characteristic of a single ZnO nanowire obtained by a wet method and contacted by EBL.

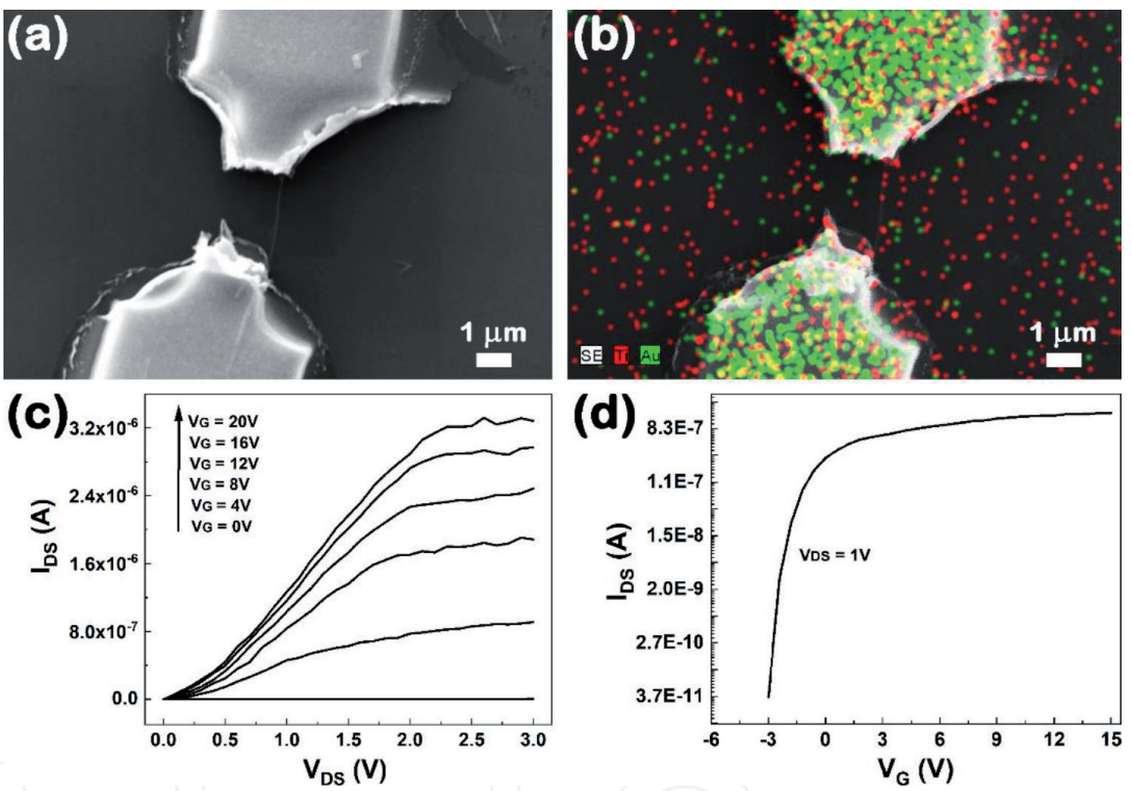


Figure 15.
(a) SEM image, (b) EDX elemental mapping, (c) output and (d) transfer characteristics of a FET based on a single ZnO nanowire obtained by a wet method and contacted by EBL.

the presence of the Ti and Au elements into the source and drain electrodes provided by EBL.

The output characteristics of a FET based on a single ZnO nanowire (**Figure 13(c)**) evidence an increase in the source-drain current towards higher positive gate voltages, typical for an n-type semiconductor channel. It can be observed that at 1.5 V applied drain-source voltage, the FET reaches the saturation region. The semilogarithmic plot of the transfer characteristic of a FET having a single ZnO nanowire as a channel (**Figure 13(d)**) exhibits an I_{ON}/I_{OFF} ratio $\approx 10^5$, in accordance with data reported in the literature for FETs based on single nanowires [13].

In the following, single ZnO nanowires synthesized by a wet technique were used as n-type channels into FET devices. Accordingly, FETs based on single ZnO nanowires were developed by contacting single ZnO nanowires at both ends with Ti/Au (100 nm/200 nm) by EBL, RF magnetron sputtering and thermal vacuum evaporation. **Figure 14(a)** reveals the SEM image of a single ZnO nanowire

synthesized by a wet method contacted by EBL. Similar to the ZnO nanowires prepared by a dry path, the current–voltage characteristic of a single ZnO nanowire obtained by a wet approach contacted by EBL (**Figure 14(b)**) exhibits a linear shape, with an Ohmic contact between the ZnO nanowire and the two Ti/Au contacts.

The SEM image at a higher magnification of a single ZnO nanowire contacted by EBL (**Figure 15(a)**) evidences that the length of the nanowire channel between the source and drain is about 2 μm. The corresponding EDX mapping image (**Figure 15(b)**) confirms the presence of the Ti and Au elements into the source and drain metallic electrodes fabricated by EBL.

The output characteristics of a FET based on a single ZnO nanowire prepared by a wet method (**Figure 15(c)**) disclose an increase in the source-drain current towards higher positive gate voltages, demonstrating that the channel is an n-type semiconductor. In addition, it can be noticed that at 2 V applied drain-source voltage, the FET reaches the saturation region. The semilogarithmic plot of the transfer characteristic of a FET having a single ZnO nanowire as an n-type channel (**Figure 15(d)**) reveals an I_{ON}/I_{OFF} ratio $\approx 10^4$, the value being in accordance with data reported in the literature for ZnO single nanowires based FETs [13].

5. Conclusions

Metal oxide, ZnO and CuO, nanowire arrays were obtained by using two straightforward and cost-effective preparation methods: chemical synthesis in aqueous solution (wet) and thermal oxidation in air (dry). The influence of the preparation technique on the morphological, structural and optical properties of the metal oxide nanowire arrays were investigated. Further, ZnO and CuO nanowires prepared by these wet and dry approaches were successfully integrated as active elements into electronic devices, such as Schottky diodes and FETs by using lithographic techniques (photolithography, EBL and FIBID) and thin film deposition techniques (RF magnetron sputtering and thermal vacuum evaporation). Additionally, the characteristic parameters for the diodes and FETs were estimated from the electrical measurements: $n \approx 1.8$ and I_{ON}/I_{OFF} ratio $\approx 10^3$ for diodes and I_{ON}/I_{OFF} ratio $\approx 10^4$–10^5 for the FETs.

The main advantage of fabricating electronic devices based on single metal oxide nanowires is represented by the possibility to integrate them in optoelectronic applications.

Acknowledgements

This work has been funded by the Executive Agency for Higher Education, Research, Development and Innovation Funding (UEFISCDI), Romania, Project code: Project code: PN-III-P1-1.1-PD-2019-1102 and by the Core Program, contract no. PN19-03 (contract no. 21 N/08.02.2019) supported from the Romanian Ministry of Research and Innovation.

Conflict of interest

The authors declare no conflict of interest.

IntechOpen

IntechOpen

Author details

Andreea Costas*, Nicoleta Preda, Camelia Florica and Ionut Enculescu
National Institute of Materials Physics, Multifunctional Materials and Structures Laboratory, Functional Nanostructures Group, Magurele, Ilfov, Romania

*Address all correspondence to: andreea.costas@infim.ro

IntechOpen

© 2020 The Author(s). Licensee IntechOpen. This chapter is distributed under the terms of the Creative Commons Attribution License (http://creativecommons.org/licenses/by/3.0), which permits unrestricted use, distribution, and reproduction in any medium, provided the original work is properly cited. CC BY

References

[1] Pan H., Feng Y. P. Semiconductor nanowires and nanotubes: Effects of size and surface-to-volume ratio. ACS Nano. 2008;2:2410-2414. DOI: 10.1021/nn8004872

[2] Wang Z., Nabet B. Nanowire Optoelectronics. Nanophotonics. 2015;1:491-502. DOI: 10.1515/nanoph-2015-0025

[3] Prashanthi K., Thundat T. Nanowire Sensors Using Electrical Resonance. Journal of The Electrochemical Society. 2020;167:037538. DOI: 10.1149/1945-7111/ab67a2

[4] Tian Y., Bakaula S. R., Wu T. Oxide nanowires for spintronics: materials and devices. Nanoscale. 2012;4:1529-1540.

[5] Zeng Z., Yan Y., Chen J., Zan P., Tian Q., Chen P. Boosting the Photocatalytic Ability of Cu_2O Nanowires for CO_2 Conversion by MXene Quantum Dots. Advanced Functional Materials. 2019;29:1806500. DOI: 10.1002/adfm.201806500

[6] Katwal G., Rao B. M., Varghese O. K. 1D oxide nanostructures based chemical sensors for noninvasive medical diagnosis. IEEE Sensors. 2016. DOI: 10.1109/ICSENS.2016.7808404

[7] Martínez-Banderas A. I., Aires A., Quintanilla M., Holguín-Lerma J. A., Lozano-Pedraza C., Teran F. J., Moreno J. A., Perez J. E., Ooi B. S., Ravasi T., Merzaban J. S., Cortajarena A. L., Kosel J. Iron-Based Core–Shell Nanowires for Combinatorial Drug Delivery and Photothermal and Magnetic Therapy. ACS Applied Materials & Interfaces. 2019;11:43976-43988. DOI: 10.1021/acsami.9b17512

[8] Sun Y.-L., Sun S.-M., Wang P., Dong W.-F., Zhang L., Xu B.-B., Chen Q.-D., Tong L.-M., Sun H.-B. Customization of Protein Single Nanowires for Optical Biosensing. Small. 2015;11:2869-2876. DOI: 10.1002/smll.201401737

[9] Lin C.-H., Feng M.-H., Hwang C.-H., Wu J. Y.-S., Su P.-C., Lin M.-Y., Chen C.-H., Chen B.-H., Huang B.-Y., Luc M.-P., Yang Y.-S. Surface composition and interactions of mobile charges with immobilized molecules on polycrystalline silicon nanowires. Sensors and Actuators B: Chemical. 2015;211:7-16. DOI: 10.1016/j.snb.2015.01.052

[10] Lu M.-P., Hsiao C.-Y., Lai W.-T., Yang Y.-S. Probing the sensitivity of nanowire-based biosensors using liquid-gating. Nanotechnology. 2010;21:425505. DOI: 10.1088/0957-4484/21/42/425505

[11] Florica C., Costas A., Boni A. G., Negrea R., Ion L., Preda N., Pintilie L., Enculescu I. Electrical properties of single CuO nanowires for device fabrication: Diodes and field effect transistors. Applied Physics Letters. 2015;106:223501. DOI: 10.1063/1.4921914

[12] Florica C., Matei E., Costas A., Toimil Molares M. E., Enculescu I. Field effect transistor with electrodeposited ZnO nanowire channel. Electrochimica Acta. 2014;137:290-297. DOI: 10.1016/j.electacta.2014.05.124

[13] Florica C., Costas A., Kuncser A., Preda N., Enculescu I. High performance FETs based on ZnO nanowires synthesized by low cost methods. Nanotechnology. 2016;27:475303. DOI: 10.1088/0957-4484/27/47/475303

[14] Chen M., Mu L., Wang S., Cao X., Liang S., Wang Y., She G., Yang J., Wang Y., Shi W. A Single Silicon Nanowire-Based Ratiometric Biosensor for Ca^{2+} at Various Locations in a Neuron. ACS Chemical Neuroscience.

2020;11:1283-1290. DOI: 10.1021/acschemneuro.0c00041

[15] Costas A., Florica C., Preda N., Apostol N. Kuncser A., Nitescu A., Enculescu I. Radial heterojunction based on single ZnO-Cu_xO core-shell nanowire for photodetector applications. Scientific Reports. 2019;9:5553. DOI: 10.1038/s41598-019-42060-w

[16] Zhang G., Li Z., Yuan X., Wang F., Fu L., Zhuang Z., Ren F.-F., Liu B., Zhang R., Tan H. H., Jagadish C. Single nanowire green InGaN/GaN light emitting diodes. Nanotechnology. 2016;27:435205. DOI: 10.1088/0957-4484/27/43/435205

[17] Barrigón E., Hrachowina L., Borgström M. T. Light current-voltage measurements of single, as-grown, nanowire solar cells standing vertically on a substrate. Nano Energy. 2020;78:105191. DOI: 10.1016/j.nanoen.2020.105191

[18] Enculescu I., Toimil-Molares M. E., Zet C., Daub M., Westerberg L., Neumann R., Spohr R. Current perpendicular to plane single-nanowire GMR sensor. Applied Physics A. 2007;86:43-47. DOI: 10.1007/s00339-006-3738-2

[19] Boughey F. L., Davies T., Datta A., Whiter R. A., Sahonta S.-L., Kar-Narayan S. Vertically aligned zinc oxide nanowires electrodeposited within porous polycarbonate templates for vibrational energy harvesting. Nanotechnology. 2016;27:28LT02. DOI: 10.1088/0957-4484/27/28/28LT02

[20] Kim S., Lee Y., Gu A., You C., Oh K., Lee S., Im Y. Synthesis of Vertically Conformal ZnO/CuO Core–Shell Nanowire Arrays by Electrophoresis-Assisted Electroless Deposition. The Journal of Physical Chemistry C. 2014;118:7377-7385. DOI: 10.1021/jp410293j

[21] Bae C. H., Park S. M., Ahn S.-E., Oh D.-J., Kim G. T., Ha J. S. Sol–gel synthesis of sub-50 nm ZnO nanowires on pulse laser deposited ZnO thin films. Applied Surface Science. 2006;253:1758-1761. DOI: 10.1016/j.apsusc.2006.03.006

[22] VillafuerteJ., DonatiniF., KioseoglouJ., Sarigiannidou E., Chaix-Pluchery O., Pernot J., Consonni V. Zinc Vacancy–Hydrogen Complexes as Major Defects in ZnO Nanowires Grown by Chemical Bath Deposition. The Journal of Physical Chemistry C. 2020;124:16652-16662. DOI: 10.1021/acs.jpcc.0c04264

[23] Fra V., Beccaria M., Milano G., Guastella S., Bianco S., Porro S., Laurenti M., Stassi S., Ricciardi C. Hydrothermally grown ZnO nanowire array as an oxygen vacancies reservoir for improved resistive switching. Nanotechnology. 2020;31:374001. DOI: 10.1088/1361-6528/ab9920

[24] Guo R. Q., Nishimura J., Matsumoto M., Nakamura D., Okada T. Catalyst-free synthesis of vertically-aligned ZnO nanowires by nanoparticle-assisted pulsed laser deposition. Applied Physics A. 2008;93:843. DOI: 10.1007/s00339-008-4791-9

[25] Liang Y. Chemical vapor deposition synthesis of Ge doped ZnO nanowires and the optical property investigation. Physics Letter A. 2019;383:2928-2932. DOI: 10.1016/j.physleta.2019.06.024

[26] Sultan S. M., Ditshego N. J., Gunn R., Ashburn P., Chong H. M. H. Effect of atomic layer deposition temperature on the performance of top-down ZnO nanowire transistors. Nanoscale Research Letters. 2014;9:517. DOI: 10.1186/1556-276X-9-517

[27] Garry S., McCarthy E., Mosnier J. P., McGlynn E. Control of ZnO nanowire arrays by nanosphere lithography (NSL) on laser-produced ZnO substrates. Applied Surface Science. 2011;257:5159-5162. DOI: 10.1016/j.apsusc.2010.11.182

[28] Pachauri V., Vlandas A., Kern K., Balasubramanian K. Site-Specific Self-Assembled Liquid-Gated ZnO Nanowire Transistors for Sensing Applications. Small. 2010;6:589-594. DOI: 10.1002/smll.200900876

[29] Vayssieres L. Growth of Arrayed Nanorods and Nanowires of ZnO from Aqueous Solutions. Advanced Materials. 2003;15:464-466. DOI: 10.1002/adma.200390108

[30] Jiang X., Herricks T., Xia Y. CuO Nanowires Can Be Synthesized by Heating Copper Substrates in Air. Nano Letters. 2002;2:1333-1338. DOI: 10.1021/nl0257519

[31] Su M., Zhang T., Su J., Wang Z., Hu Y., Gao Y., Gu H., Zhang X. Homogeneous ZnO nanowire arrays p-n junction for blue light-emitting diode applications. Optics Express. 2019;27:A1207–A1215. DOI: 10.1364/OE.27.0A1207

[32] Mahmoud F. A., Ahmed N. Elaboration of ZnO nanowires by solution based method, characterization and solar cell applications. Journal of Semiconductors. 2018;39:093002. DOI: 10.1088/1674-4926/39/9/093002

[33] Athauda T. J., Neff J. G., Sutherlin L., Butt U., Ozer R.R. Systematic Study of the Structure–Property Relationships of Branched Hierarchical TiO_2/ZnO Nanostructures. ACS Applied Materials & Interfaces. 2012;4:6917-6926. DOI: 10.1021/am302061z

[34] Wei Q., Meng G., An X., Hao Y., Zhang L. Temperature-controlled growth of ZnO nanostructures: branched nanobelts and wide nanosheets. Nanotechnology. 2005;16:2561. DOI: 10.1088/0957-4484/16/11/016

[35] Zhao S., Shen Y., Zhou P., Hao F., Xu X., Gao S., Wei D., Ao Y., Shen Y. Enhanced NO_2 sensing performance of ZnO nanowires functionalized with ultra-fine In_2O_3 nanoparticles. Sensors and Actuators B: Chemical. 2020;308:127729. DOI: 10.1016/j.snb.2020.127729

[36] Florica C., Costas A., Preda N., Beregoi M., Kuncser A., Apostol N., Popa C., Socol G., Diculescu V., Enculescu I. Core-shell nanowire arrays based on ZnO and Cu_xO for water stable photocatalysts. Scientific Reports. 2019;9:17268. DOI: 10.1038/s41598-019-53873-0

[37] Florica C., Preda N., Costas A., Zgura I., Enculescu I. ZnO nanowires grown directly on zinc foils by thermal oxidation in air: Wetting and water adhesion properties. Materials Letters. 2016;170:156-159. DOI: 10.1016/j.matlet.2016.02.035

[38] Naveena D. , Logu T. , Dhanabal R. , Sethuraman K. , Bose A. C. Comparative study of effective photoabsorber CuO thin films prepared via different precursors using chemical spray pyrolysis for solar cell application. Journal of Materials Science: Materials in Electronics. 2019;30:561-572. DOI: 10.1007/s10854-018-0322-4

[39] Li D., Tang Y., Ao D., Xiang X., Wang S., Zu X. Ultra-highly sensitive and selective H_2S gas sensor based on CuO with sub-ppb detection limit. International Journal of Hydrogen Energy. 2019;44:3985-3992. DOI: 10.1016/j.ijhydene.2018.12.083

[40] Jiang D., Xue J., Wu L., Zhou W., Zhang Y., Li X. Photocatalytic performance enhancement of CuO/Cu_2O heterostructures for photodegradation of organic dyes: Effects of CuO morphology. Applied Catalysis B: Environmental. 2017;211:199-204. DOI: 10.1016/j.apcatb.2017.04.034

[41] Xu Y., Ma J., Han Y., Zhang J., Cui F., Zhao Y., Li X., Wang W. Multifunctional

CuO Nanowire Mesh for Highly Efficient Solar Evaporation and Water Purification. ACS Sustainable Chemistry & Engineering. 2019;7:5476-5485. DOI: 10.1021/acssuschemeng.8b06679

[42] Wu D., Zhang Q., Tao M. LSDA +U study of cupric oxide: Electronic structure and native point defects. Physical Review B. 2006;73:235206. DOI: 10.1103/PhysRevB.73.235206

[43] Wang W., Wang L., Shia H., Liang Y. A room temperature chemical route for large scale synthesis of sub-15 nm ultralong CuO nanowires with strong size effect and enhanced photocatalytic activity. CrystEngComm. 2012;14: 5914-5922. DOI: 10.1039/C2CE25666E

[44] Shi W., Chopra N. Surfactant-free synthesis of novel copper oxide (CuO) nanowire–cobalt oxide (Co_3O_4) nanoparticle heterostructures and their morphological control. Journal of Nanoparticle Research. 2011;13:851-868. DOI: 10.1007/s11051-010-0086-0

[45] Meng J., Li Z. Schottky-Contacted Nanowire Sensors. Advanced Materials. 2020;32:2000130. DOI: 10.1002/adma.202000130

IntechOpen